

Individual dynamic predictions using landmarking and joint modelling: validation of estimators and robustness assessment

Loïc Ferrer^{1,†}, Hein Putter² and Cécile Proust-Lima¹

July 2017

¹ INSERM, UMR1219, Univ. Bordeaux, ISPED, F-33076 Bordeaux, France

² Leiden University Medical Center, Leiden, the Netherlands

† email: loic.ferrer@inserm.fr

Abstract: After the diagnosis of a disease, one major objective is to predict cumulative probabilities of events such as clinical relapse or death from the individual information collected up to a prediction time, including usually biomarker repeated measurements. Several competing estimators have been proposed to calculate these individual dynamic predictions, mainly from two approaches: joint modelling and landmarking. These approaches differ by the information used, the model assumptions and the complexity of the computational procedures. It is essential to properly validate the estimators derived from the joint models and the landmark models, quantify their variability and compare them in order to provide key elements for the development and use of individual dynamic predictions in clinical follow-up of patients. Motivated by the prediction of two competing causes of progression of prostate cancer from the history of prostate-specific antigen, we conducted an in-depth simulation study to validate and compare the dynamic predictions derived from these two methods. Specifically, we formally defined the quantity to estimate and its estimators, proposed techniques to assess the uncertainty around predictions and validated them. We also compared the individual dynamic predictions derived from joint models and landmark models in terms of accuracy of prediction, efficiency and robustness to model assumptions. We show that these prediction tools should be handled with care, in particular by properly specifying models and estimators.

Keywords: Competing risks; Dynamic Prediction; Landmarking; Joint modelling; Prediction accuracy; Robustness.

1 Introduction

After diagnosis and subsequent treatment of cancer, patients are typically monitored via repeated measurements of biomarkers. For example, in patients with prostate cancer treated by radiotherapy, the Prostate Specific Antigen (PSA) is measured routinely. Precisely predicting the individualized probabilities of events such as clinical relapse for these patients from their individual information collected until the prediction time has become a central issue (Goldstein et al., 2017; Proust-Lima and Taylor, 2009). Personalized treatment strategies can indeed be proposed according to the updated individual probabilities (Sène et al., 2016), or the planning of the next biomarker measurement can be optimized (Rizopoulos et al., 2015).

Two main approaches have been proposed to compute individual dynamic predictions: joint modelling and landmarking. These differ in the used information, the model assumptions and the complexity of computational procedures.

The *joint modelling (JM) approach* simultaneously models the repeated measurements of the biomarker (e.g., using a linear mixed model in standard JM) and the time-to-event data (e.g., using a proportional hazards model in standard JM) by linking them using a function of shared random effects (Tsiatis and Davidian, 2004). This approach has the advantage of only requiring one model estimation for any prediction time, and of modelling the progression of the disease as a whole, which makes it very popular. But it is often based on simplifying assumptions (e.g., proportional hazards, number of random effects) and may be complex to estimate, so that it should be handled carefully and can remain difficult to apply in practice.

The *landmarking approach* consists of adjusting standard survival models considering only the subsample of subjects still at risk at the prediction time and the longitudinal information collected up to the prediction time (Van Houwelingen, 2007). These models induce significantly less numerical problems and reduce the possible estimation bias related to the proportional hazards assumption. However, as they do not fully explore the collected information during the follow-up and the correlation between the marker and the time of event, they can produce sub-efficient estimators (Huang et al., 2016) and are only an approximation of the (correct) joint estimator. Indeed, as supported in Suresh et al. (2017) they do not satisfy the consistency condition introduced by Jewell and Nielsen (1993) which stipulates that the hazard function and the marker dynamics must be linked at all time points to give consistent dynamic predictions. In the presence of longitudinal biomarkers, the landmark approach can result in several models. Most of the time a survival model (cause-specific proportional hazards) is adjusted on the last observed value of the biomarker. In addition to truncation at the prediction time, censoring is administered at the end of the prediction window to reduce possible bias related to the proportionality of hazards. But this approach does not take into account fluctuations of the biomarker, its observation at discrete times and measurement errors. To circumvent this problem, the last observed value of the biomarker may be replaced by its predicted value at the prediction time (obtained from a linear mixed model) (Sweeting et al., 2016). This two-step model considers the same method of truncation and administrative censoring. It takes into account all the collected information of the biomarker until the prediction time for the subjects at risk. But the event probabilities must be deduced by approximation and the model is not completely freed of the proportional hazards assumption. In the context of competing risks, rather than using a cause-specific proportional hazards model, the conditional probabilities of event can be directly estimated by a dynamic pseudo-observations approach (Nicolaie et al., 2013). This approach directly models the conditional probabilities of event and is freed from the proportionality hazards assumption. By considering the predicted value of the biomarker at the prediction time as a covariate, it also takes into account the trajectory of the biomarker. But this approach requires the spec-

ification of a link function and can still provide less efficient estimators than the joint model. Note that, in these landmark models as well as in joint models, any function of the biomarker trajectory parameters can be used instead of the biomarker predicted value at the prediction time. In addition, although of central interest in many recent works, estimators of dynamic predictions and of their uncertainty were never formally validated while there exist several competing proposals in the joint modelling framework (Rizopoulos, 2011; Sène et al., 2016). In the landmarking approach, some estimators were proposed when including only baseline information but not when including also longitudinal biomarkers and no estimator of the variability was ever proposed.

Motivated by the prediction of competing progressions of prostate cancer from the PSA history, we first proposed estimators of individual dynamic predictions and of their uncertainty with 95% confidence intervals for the joint and the landmark approaches, and we properly validated them. We then compared the predictive accuracy of the models under several scenarios to explore their robustness to misspecification.

The rest of the paper is organized as follows. Section 2 introduces the prediction models and the derived estimators of dynamic predictions and of their uncertainty. Section 3 briefly describes the motivating data. The simulation studies are carried out in Section 4 for validating the proposed estimators and comparing them in terms of prediction accuracy. The paper ends with a discussion in Section 5.

2 Prediction models

Let us consider the competing risks setting where the subjects are at risk to experience K competing events. For each subject i ($i = 1, \dots, N$), we denote T_i the earliest time-to-event and $\delta_i = k$ the cause of event, with $k \in 1, \dots, K$. In the presence of censoring, we observe the event time $T_i^\dagger = \min(T_i, C_i)$ with C_i the censoring time, and the indicator of event becomes $\Delta_i = \delta_i \cdot \mathbb{1}\{T_i \leq C_i\}$ with $\mathbb{1}$ the indicator function. We also observe X_i the vector of baseline covariates and Y_i a longitudinal marker measured repeatedly with $Y_i(t_{ij})$ the observed measure at time t_{ij} for $j = 1, \dots, n_i$ and $t_{in_i} \leq T_i^\dagger$. In the following, $\mathcal{Y}_i(s) = \{Y_i(t_{ij}) : 0 \leq t_{ij} \leq s, j = 1, \dots, n_i(s)\}$ denotes the history of the marker until time s and the model formulations assume a longitudinal marker with Gaussian distribution.

In this paper we are interested in the individual cumulative probability of the event of cause k between times s and $s + w$ for a new subject \star , with s the landmark time (or prediction time) and w the horizon. This probability, also called landmark specific cumulative incidence of cause k is defined as

$$\pi_\star^k(s, w) = \Pr(s < T_\star \leq s + w, \delta_\star = k | T_\star > s, \mathcal{Y}_\star(s), X_\star). \quad (1)$$

We focus on several parametric models from which an estimator of the landmark specific cumulative incidence of cause k can be derived:

$$\widehat{\pi}_\star^k(s, w; \widehat{\theta}) = \Pr(s < T_\star \leq s + w, \delta_\star = k | T_\star > s, \mathcal{Y}_\star(s), X_\star, \mathcal{I}; \widehat{\theta}), \quad (2)$$

with $\widehat{\theta}$ the vector of parameters estimated on the observed data called \mathcal{I} in the remainder of the manuscript.

2.1 Joint model

2.1.1 Model formulation

The joint model considers the full collected information $\mathcal{I} = \{(T_i^\dagger, \Delta_i, \mathcal{Y}_i(T_i^\dagger), X_i); i = 1, \dots, N\}$. It is decomposed into two sub-models linked by a function of a shared latent structure. The most popular joint model (Rizopoulos, 2012) links a linear mixed model for the repeated measurements of the marker

and a cause-specific proportional hazards model for the specific hazard of each cause of event k using a function of shared random effects:

$$\begin{cases} Y_i(t) &= m_i(t) + \epsilon_i(t) \\ &= X_i^L(t)^\top \beta + Z_i(t)^\top b_i + \epsilon_i(t), \\ \lambda_i^k(t) &= \lambda_{k,0}(t) \exp \left\{ X_{k,i}^E \gamma_k + W_{k,i}(t|b_i; \beta)^\top \eta_k \right\}, \end{cases}$$

where $t > 0$ and $\lambda_i^k(t)$ denotes the hazard function of cause k at time t , with $k = 1, \dots, K$. In the longitudinal sub-part, $X_i^L(t)$ and $Z_i(t)$ denote vectors of covariates (possibly time-dependent) associated respectively with the vector of fixed effects β and the vector of random effects b_i , $b_i \sim \mathcal{N}_q(0, D)$. The error term is $\epsilon_i(t) \sim \mathcal{N}(0, \sigma^2)$; the random effects and error terms are independent. In the survival sub-part, $\lambda_{k,0}(t)$ denotes the parametric baseline hazard of cause k at time t . The vector of covariates $X_{k,i}^E$ is associated with the vector of coefficients γ_k . The (possibly multivariate) function $W_{k,i}(t|b_i; \beta)$ denotes the function of dependence between the longitudinal process and the hazard of event of cause k , such as for example the unbiased current level of the marker $m_i(t)$, the unbiased current slope $\partial m_i(t)/\partial t$, or both $(m_i(t), \partial m_i(t)/\partial t)^\top$.

The joint model assumes proportional hazards (PH) between levels of covariates.

It can be estimated in the maximum likelihood framework by using the independence between the longitudinal process $\mathcal{Y}_i(T_i^\dagger)$ and the survival process (T_i^\dagger, Δ_i) conditionally on the random effects b_i . The likelihood involves integrals over the random effects and time that have to be numerically solved, usually using Gaussian quadratures. Note that the number of quadrature points has to be chosen carefully to provide correct inference (Ferrer et al., 2016).

2.1.2 Cumulative incidence estimator

Once the model is estimated, the vector of parameters $\widehat{\theta}$ and its variance matrix $\widehat{V(\theta)}$ are obtained and we are able to compute for each new subject \star the predicted conditional cumulative incidence of cause k for all the possible horizons w and landmark times s :

$$\widehat{\pi}_\star^k(s, w; \widehat{\theta}) = \int_{\mathbb{R}^q} \Pr(s < T_\star \leq s + w, \delta_\star = k | T_\star > s, X_\star, b_\star, \widehat{\theta}) f(b_\star | T_\star > s, \mathcal{Y}_\star(s), X_\star; \widehat{\theta}) db_\star. \quad (3)$$

Another estimator of (2) (faster but less accurate) can be obtained by replacing the integration over the random effect distribution by a punctual computation at a predicted value of the random effects. It is called the conditional prediction. The complete formulas of the marginal and conditional probabilities are detailed in Sections 1.1 and 1.2 of the Web Appendix.

We propose to derive a 95% confidence interval of (3) using parametric bootstrap techniques. The procedure is realized as follows:

Consider a large L ; for each $l = 1, \dots, L$,

1. generate $\widetilde{\theta}^{(l)} \sim \mathcal{N}(\widehat{\theta}, \widehat{V(\theta)})$;
2. compute $\widetilde{\pi}_\star^{k,(l)}(s, w; \widetilde{\theta}^{(l)}) = \int_{\mathbb{R}^q} \Pr(s < T_\star \leq s + w, \delta_\star = k | T_\star > s, X_\star, b_\star; \widetilde{\theta}^{(l)}) f(b_\star | T_\star > s, \mathcal{Y}_\star(s), X_\star; \widetilde{\theta}^{(l)}) db_\star$.

The same technique can be used with the conditional estimator of the probability by replacing the expression in step 2.

The 95% confidence interval is defined by the 2.5th and 97.5th percentiles of $\{\tilde{\pi}_{\star}^{k,(l)}(s, w; \tilde{\theta}^{(l)}); l = 1, \dots, L\}$. These techniques are validated in Section 4.1.

Note that our proposal differs from an existing technique that additionally bootstraps the random effects (Rizopoulos, 2011). We compared both techniques in Section 2 of the Web Appendix and show that only the parameters θ (as done here) should be bootstrapped to provide correct inference.

2.2 Landmark cause-specific proportional hazards model

An alternative to joint models is landmark models which only consider subjects at risk at a landmark time s and the longitudinal information $\{\mathcal{Y}(s), X\}$ collected until s . When considering PH landmark models, administrative censoring is applied at the end of the prediction window $s + w$ in order to reduce the possible bias entailed by a violation of the PH assumption. The considered information becomes $\mathcal{I} = \{(\xi_i(s, w), \Psi_i(s, w), \mathcal{Y}_i(s), X_i); i = 1, \dots, N^{\dagger}(s)\}$, with $\xi_i(s, w) = \min(T_i^{\dagger}, s + w)$, $\Psi_i(s, w) = \Delta_i \cdot \mathbb{1}\{s < T_i \leq s + w\}$ and $N^{\dagger}(s) = \sum_{i=1}^N \mathbb{1}\{T_i^{\dagger} > s\}$.

2.2.1 Model formulation

The landmark cause-specific (CS) proportional hazards (PH) model is defined by

$$\lambda_i^k(t) = \lambda_{k,0}(t) \exp \left\{ X_{k,i}^E \gamma_k + W_{k,i}(s)^{\top} \eta_k \right\},$$

where $t > s$, $\lambda_{k,0}(\cdot)$ is an unspecified cause-specific baseline hazard function and $W_{k,i}(s)$ is a multivariate function that depicts the dynamics of the marker extrapolated at time s . The model is estimated by maximizing the Cox partial likelihood (Cox, 1972) for each considered pair of landmark and horizon times. Note that for the sake of clarity, we did not use a subscript s, w for the model parameters although they are different for each (s, w) .

To take into account the information of the marker before the landmark time s , one can consider the last observed value only, i.e. $W_{k,i}(s) = Y_i(t_{in_i(s)})$. However, this technique, called "naive landmark model" assumes that the marker is measured without error and considers neither the whole trajectory of the marker until s nor the subject-specific gap between $t_{in_i(s)}$ and s .

A better alternative is to deduce the value of $W_{k,i}(s)$ at time s from a linear mixed model estimated on the marker measurements collected until s in subjects at risk at s . This technique, called the "two-stage landmark model" considers $W_{k,i}(s) = \widehat{W}_{k,i}(s|\widehat{b}_i; \widehat{\beta})$, where $\widehat{\beta}$ is the vector of estimated fixed effects and $\widehat{b}_i = \mathbb{E}(b_i | \mathcal{Y}_i(s), X_i; \widehat{\theta}) = \widehat{D}Z_i^{\top} \widehat{V}_i^{-1} (Y_i - X_i^L \widehat{\beta})$ is the vector of empirical Bayes estimates of the individual random effects, with $\widehat{V}_i = Z_i \widehat{D}Z_i^{\top} + \widehat{\sigma}^2 I_{n_i(s)}$. Here X_i^L and Z_i are the matrices of covariates with respectively the row vectors $X_i^L(t_{ij})^{\top}$ and $Z_i(t_{ij})^{\top}$, and the column vector Y_i is with elements Y_{ij} , for $j = 1, \dots, n_i(s)$. I is the identity matrix.

2.2.2 Cumulative incidence estimator

With the two-stage approach, the predicted conditional cumulative incidence of cause k for subject \star is

$$\tilde{\pi}_{\star}^k(s, w; \widehat{\theta}) = \Pr(s < T_{\star} \leq s + w, \delta_{\star} = k | T_{\star} > s, X_{\star}, \widehat{b}_{\star}; \widehat{\theta}), \quad (4)$$

where $\widehat{\theta}$ is the vector of estimated parameters (with associated estimated variance $\widehat{V}(\widehat{\theta})$), and $\widehat{b}_{\star} = \mathbb{E}(b_{\star} | \mathcal{Y}_{\star}(s), X_{\star}; \widehat{\theta})$.

To estimate valid 95% confidence intervals, it is necessary to take into account the variability due to the parameter and baseline hazard estimates. The same parametric bootstrap technique as described

for the joint model can be used for the parameter estimates but it can't be applied for the baseline hazard estimates. The unspecified cumulative baseline hazard $\Lambda_{k,0}(t) = \int_s^t \lambda_{k,0}(u) du$ is estimated using the Breslow's estimator (Breslow, 1972), $\widehat{\Lambda}_{k,0}(t) = \int_s^t \widehat{\Pi}_k^{(0)}(\widehat{\theta}, u)^{-1} d\bar{J}_k(u)$ where $\widehat{\Pi}_k^{(0)}(\widehat{\theta}, u) = \frac{1}{N^\dagger(s)} \sum_{i=1}^{N^\dagger(s)} \mathbb{1}\{\xi_i(s, w) \geq u\} \exp\{X_{k,i}^E \gamma_k + \widehat{W}_{k,i}(s|\widehat{b}_i; \widehat{\beta})^\top \widehat{\eta}_k\}$ and $\bar{J}_k(u) = \frac{1}{N^\dagger(s)} \sum_{i=1}^{N^\dagger(s)} \mathbb{1}\{\xi_i(s, w) \leq u, \Psi_i(s, w) = k\}$. Thus we propose a procedure that combines parametric bootstrap to take into account the variability associated to $\widehat{\theta}$ and perturbation-resampling methods, inspired by Sinnott and Cai (2016), to take into account the variability associated to $\widehat{\Lambda}_{k,0}(.)$.

This technique, which also avoids hard computational cost, is validated in the simulation study in Section 4.1. The full procedure is realized as follows:

For each bootstrap sample $l = 1, \dots, L$, where L is large enough;

1. generate $\widetilde{\theta}^{(l)} \sim \mathcal{N}(\widehat{\theta}, V(\widehat{\theta}))$ and deduce $\widetilde{b}^{(l)} = \mathbb{E}(b | \mathcal{Y}_l(s), X_l; \widetilde{\theta}^{(l)})$;
2. for each subject $i \in 1, \dots, N^\dagger(s)$ of the learning sample, generate $v_i^{(l)} \sim 4 \cdot \text{Beta}(1/2, 3/2)$;
3. compute $\widetilde{\Lambda}_{k,0}^{(l)}(t) = \int_s^t \widetilde{\Pi}_k^{(0), (l)}(\widetilde{\theta}^{(l)}, u)^{-1} d\bar{J}_k^{(l)}(u)$ with $\widetilde{\Pi}_k^{(0), (l)}(\widetilde{\theta}^{(l)}, u) = \frac{1}{N^\dagger(s)} \sum_{i=1}^{N^\dagger(s)} v_i^{(l)} \mathbb{1}\{\xi_i(s, w) \geq u\} \exp\{X_{k,i}^E \gamma_k^{(l)} + \widehat{W}_{k,i}(s|\widehat{b}_i^{(l)}; \widetilde{\theta}^{(l)})^\top \widehat{\eta}_k^{(l)}\}$ and $\bar{J}_k^{(l)}(u) = \frac{1}{N^\dagger(s)} \sum_{i=1}^{N^\dagger(s)} v_i^{(l)} \mathbb{1}\{\xi_i(s, w) \leq u, \Psi_i(s, w) = k\}$;
4. for each subject \star of the validation sample, deduce $\widetilde{\pi}_{\star}^{k, (l)}(s, w; \widetilde{\theta}^{(l)}) = f(\{(\widetilde{\Lambda}_{k,0}^{(l)}(u), s < u \leq s + w); k = 1, \dots, K\}, \widetilde{\theta}^{(l)}, \widetilde{b}_{\star}^{(l)})$, where $f(.)$ is a function specified in Section 1.4 of the Web Appendix.

We can obtain the 95% confidence interval by considering the 2.5th and 97.5th percentiles of $\{\widetilde{\pi}_{\star}^{k, (l)}(s, w; \widetilde{\theta}^{(l)}); l = 1, \dots, L\}$.

Using a naive approach, the predicted conditional cumulative incidence of cause k for subject \star is

$$\widehat{\pi}_{\star}^k(s, w; \widehat{\theta}) = \Pr(s < T_{\star} \leq s + w, \delta_{\star} = k | T_{\star} > s, X_{\star}, Y_{\star}(t_{\star n_{\star}(s)}); \widehat{\theta}), \quad (5)$$

and the same technique combining parametric bootstrap and perturbation-resampling can be used to obtain 95% confidence intervals.

2.3 Landmark model based on pseudo-observations

Cause-specific hazard models rely on the PH assumption and require the computation of integrals over time in the individual cumulative incidences. To avoid these issues, some authors have focused on the direct modelling of the individual cumulative incidences with for example the Fine-Gray model (Fine and Gray, 1999), the binomial regression models (Scheike et al., 2008) or the pseudo-value approach (Andersen and Pohar Perme, 2010). The latter is developed here. The pseudo-observation approach does not require the PH assumption, hence the considered information is $\mathcal{I} = \{(T_i^\dagger, \Delta_i, \mathcal{Y}_i(s), X_i); i = 1, \dots, N^\dagger(s)\}$.

2.3.1 Model formulation

For subjects at risk at time s , we are interested in the expectation of $\mu_i^k(s, w) = \mathbb{1}(T_i \leq s + w, \delta_i = k)$. In presence of censoring, this quantity is not always observable. Thus the idea is to define the dynamic jackknife pseudo-observation (Nicolae et al., 2013) of the non-parametric estimator of $\pi^k(s, w)$: $\widehat{\mu}_i^k(s, w) = N^\dagger(s)\widehat{F}^k(s, w) - (N^\dagger(s) - 1)\widehat{F}_{(-i)}^k(s, w)$, where $N^\dagger(s)$ is the number of subjects at risk at s and $\widehat{F}^k(s, w)$ is the Aalen-Johansen estimate of $\pi^k(s, w)$ (Andersen et al., 1993).

To include the dynamic information on the marker until s , the same two-stage approach as defined in section 2.2 can be used to deduce $\widehat{W}_{k,i}(s|\widehat{b}_i; \widehat{\beta})$ in those still at risk in s . The pseudo-observation and the prognostic factors are then linked using a model and a link function g :

$$g\left[\mathbb{E}\{\widehat{\mu}_i^k(s, w)|T_i^\dagger > s\}\right] = \gamma_{0,k} + X_{k,i}^{E^\top} \gamma_{1,k} + \widehat{W}_{k,i}(s|\widehat{b}_i; \widehat{\beta})^\top \eta_k.$$

The model is estimated using generalized estimating equations (GEE).

2.3.2 Cumulative incidence estimator

The predicted conditional cumulative incidence can directly be expressed as

$$\widehat{\pi}_\star^k(s, w; \widehat{\theta}) = \Pr(s < T_\star \leq s + w, \delta_\star = k|T_\star > s, X_\star, \widehat{b}_\star; \widehat{\theta}), \quad (6)$$

with $\widehat{b}_\star = \mathbb{E}(b_\star|\mathcal{Y}_\star(s), X_\star; \widehat{\theta})$, where $\widehat{\theta}$ is the vector of estimated parameters (with associated estimated variance matrix $V(\widehat{\theta})$). For example with the cloglog link function g ($g(x) = \text{cloglog}(x) = \log(-\log(1 - x))$), it can be expressed as: $\widehat{\pi}_\star^k(s, w; \widehat{\theta}) = 1 - \exp\left[-\exp\{\widehat{y}_{0,k} + X_{k,i}^{E^\top} \widehat{\gamma}_{1,k} + \widehat{W}_{k,i}(s|\widehat{b}_i; \widehat{\beta})^\top \widehat{\eta}_k\}\right]$.

The 95% confidence intervals may be calculated using parametric bootstrap:

Consider a large L ; for each $l = 1, \dots, L$,

1. generate $\widetilde{\theta}^{(l)} \sim \mathcal{N}(\widehat{\theta}, V(\widehat{\theta}))$ and deduce $\widetilde{b}_\star^{(l)} = \mathbb{E}(b_\star|\mathcal{Y}_\star(s), X_\star; \widetilde{\theta}^{(l)})$;
2. compute $\widetilde{\pi}_\star^{k,(l)}(s, w; \widetilde{\theta}^{(l)}) = \widetilde{\pi}_\star^{k,(l)}(s, w|\widetilde{b}_\star^{(l)}; \widetilde{\theta}^{(l)})$.

Thus we can deduce the 95% confidence interval by considering the 2.5th and 97.5th percentiles of $\{\widetilde{\pi}_\star^{k,(l)}(s, w; \widetilde{\theta}^{(l)}); l = 1, \dots, L\}$.

2.4 Implementation

The estimation of the prediction models and the computation of the derived estimators were performed in R using standard packages and extensions coded by the authors, with the `JM` package for the joint model, the `survival` package for the landmark cause-specific proportional hazards models and the `pseudo` and `geepack` packages for the landmark model based on pseudo-values. Examples of codes used for the manuscript writing can be found in Section 6 of the Web Appendix, and detailed examples can be found at <https://github.com/LoicFerrer> for practical use.

3 Motivating data

The paper relies on simulation studies inspired by the data analyzed in Ferrer et al. (2016). In this study, patients ($N = 1474$) had a clinically localized prostate cancer and were treated by external beam radiotherapy. After the end of the radiotherapy, repeated measurements of the Prostate Specific Antigen

(PSA) were collected until the occurrence of a clinical event defined as the recurrence of the disease (local/distant recurrence, initiation of hormonal therapy or death due to the prostate cancer) or death due to an other cause. Post-treatment PSA trajectory was mostly biphasic with a short term drop followed by a stable or slight increase (Proust-Lima et al., 2008). Several authors (Proust-Lima and Taylor, 2009; Taylor et al., 2013) showed that including these post-treatment PSA dynamics in dynamic prediction tools of disease recurrence highly reduced the prediction error.

4 Simulation studies

Two simulation studies were performed, one for the validation of the estimators and their variability (section 4.1), and a second for their comparison and the assessment of their robustness to misspecification (section 4.2). Both simulation studies relied on the same following design.

$R = 500$ learning samples of $N = 1000$ subjects as well as a validation sample of $N^{\text{new}}(0) = 500$ subjects were generated from a joint model (Crowther and Lambert, 2013; Ferrer et al., 2016). The models detailed in section 2 were estimated on each learning sample r ($r = 1, \dots, R$) and the derived estimators of cumulative incidence were computed for a given horizon w on the $N^{\text{new}}(s)$ subjects ($\star = 1, \dots, N^{\text{new}}(s)$) of the validation sample who did not experience any event before landmark time s .

For each replicate r , we then compared the true generated cumulative incidence $\pi_{\star}^k(s, w; \theta) = \int_{\mathbb{R}^q} \pi_{\star}^k(s, w|b_{\star}; \theta) f(b_{\star}|T_{\star} > s, \mathcal{Y}_{\star}(s), X_{\star}; \theta) db_{\star}$ with the estimators $\widehat{\pi}_{\star, r}^k(s, w; \widehat{\theta})$.

4.1 Simulation study I : Validation of the estimators $\widehat{\pi}_{\star}^k(s, w; \widehat{\theta})$

To validate the proposed estimators, we checked the distributions over the individuals of the estimated relative bias and the estimated coverage rates for $\pi_{\star}^k(s, w; \theta)$. We also investigated the efficiency of the estimators with the mean relative change in the confidence interval widths.

4.1.1 Model specification

For each subject i (learning or validation sample), data were generated according to the joint model:

$$\begin{cases} Y_i(t) &= m_i(t) + \epsilon_i(t) \\ &= (\beta_0 + \beta_{0,X}X_i + b_{i0}) + (\beta_1 + \beta_{1,X}X_i + b_{i1})t + \epsilon_i(t), \\ \lambda_i^k(t) &= \lambda_{k,0}(t) \exp \left\{ \gamma_k X_i + \eta_{1,k} m_i(t) + \eta_{2,k} \frac{\delta m_i(t)}{\delta t} \right\}, \end{cases}$$

where $\log(\lambda_{k,0}(t))$ is a combination of cubic B-splines with one internal knot, k is the cause of event (Recurrence ; Death); X_i is a continuous variable. The coefficients and the distribution of the covariates used for the generation data correspond to those obtained on the motivating data. They are given in Section 4.1 of the Web Appendix.

4.1.2 Results

Due to the duration of the procedures, the simulations were run for two landmark times $s = 1, 5$, one horizon time $w = 3$ and 200 subjects randomly selected from the validation sample. $R = 499$ and $R = 486$ replicates were considered for $s = 1$ and $s = 5$ respectively, due to convergence problems in the landmark model estimation.

Figures 1a and 1b depict respectively the distribution over the subjects of the relative bias of the estimator and the coverage rates of its 95% confidence interval both for the joint and two-stage landmark CS PH models for landmark times $s = 1$ and $s = 5$ and one horizon time $w = 3$. The box plots highlight the correct estimation of $\pi_{\star}^k(s, w; \theta)$, except for the conditional expression from the joint model in the earlier landmark times ($s = 1$). This confirms that considering the modes of the distributions a posteriori of the random effects (defined in Section 1.2 of the Web Appendix) in the conditional estimator is valid only when there is enough longitudinal information. The coverage rates which are very close to 0.95 validate the proposed 95% confidence interval computations for both approaches. Finally the comparison of the widths of the 95% confidence intervals according to the joint and two-stage landmark CS PH models (Figure 1c) underlines that the joint model estimator is much more efficient than the landmark CS PH estimator. This result was expected, because the included information in the landmark models is lower than the one in the joint model. We provide in Section 2 of the Web appendix the same graphs in standard survival context ($K = 1$) to compare our proposal for the 95% confidence interval in the joint model with the one proposed previously in Rizopoulos (2011). We show that the latter provides systematically coverage rates of 100%, and width of 95% confidence intervals that are two to five times too large. This is due to the unnecessary additional variability of the random effects considered in this technique.

[Figure 1 about here.]

4.2 Simulation study II : Robustness to models hypotheses

The second simulation study aimed to compare the proposed models in terms of prediction accuracy and robustness to the models hypotheses. We considered four scenarios: correct specification of the joint model, misspecification of the dependence function, violation of the proportional hazards assumption, and misspecification of the longitudinal trajectory of the marker. The distribution of the covariates and the coefficients used for the generation data in the four cases can be found in Section 4 of the Web Appendix.

We compared the prediction models two by two using boxplots of the differences of Mean Square Error of prediction (MSE) over the R replicates, where $\text{MSE}_r^k(s, w) = \frac{1}{N^{\text{new}}(s)} \times \sum_{\star=1}^{N^{\text{new}}(s)} (\pi_{\star}^k(s, w; \theta) - \widehat{\pi}_{\star, r}^k(s, w; \widehat{\theta}))^2$. For a given replicate r and a given landmark time s , the models were considered only if they all converged.

4.2.1 Case 1: Correct specification of the joint model

For the well-specified case, data generation and specification of the joint and landmark models in the estimation and prediction steps were the same as in Section 4.1.

Figure 2 shows differences of MSE for 8 pairs of landmark and horizon times ($s = 1, 3, 5, 8$ and $w = 1.5, 3$). As expected, the joint model performed better than the landmark models for all the pairs (s, w) . Once again, the joint model that considers the conditional probability was much worse than the marginal one in the earliest landmark times, but the estimations obtained from the two techniques were almost the same from $s = 5$. It can be noted that the convergence problems in the model estimations usually arose from insufficient considered information in landmarking.

[Figure 2 about here.]

4.2.2 Case 2: Misspecification of the dependence function

To consider a misspecification of the dependence structure, the generated data were the same as in case 1 but the prediction models neglected the slope of the marker in the estimation and prediction steps. Note that the latter had a strong impact on the risk of recurrence.

The distributions over the replicates of the differences of MSE for all the selected pairs of landmark and horizon times are depicted in Figure 3. Relative to the marginal estimator from the joint model, the other estimators behave similarly as in case 1. Mainly, the joint model remains better than the landmark models. However, neglecting the slope in the dependence structure induced a large increase in the MSE of the marginal estimator from the joint model which is provided in each graph in Figure 3 and Figure 2; for instance, for $(s, w) = (1, 3)$, the MSE increases from 0.323 to 1.114 when neglecting the slope in the dependence structure. This underlines the great importance of correctly specifying the dependence function in these models.

[Figure 3 about here.]

4.2.3 Case 3: Violation of the proportional hazards assumption

The robustness of the models when the proportional assumption is violated was checked by considering an interaction with $\log(1 + t)$ for the parameters associated with the marker dynamics in the generation model:

$$\begin{cases} Y_i(t) &= m_i(t) + \epsilon_i(t) \\ &= (\beta_0 + \beta_{0,X}X_i + b_{i0}) + (\beta_1 + \beta_{1,X}X_i + b_{i1})t + \epsilon_i(t), \\ \lambda_i^k(t) &= \lambda_{k,0}(t) \exp \left\{ \gamma_k X_i + \eta_{1,k} \log(1 + t) m_i(t) + \eta_{2,k} \log(1 + t) \frac{\delta m_i(t)}{\delta t} \right\}. \end{cases}$$

For all the prediction models, the estimation and prediction steps did not consider this interaction with $\log(1 + t)$.

Boxplots of the differences of MSE over the replicates are depicted in Figure 4. Even under this strong violation of the PH assumption, the performances of the two-stage landmark and joint models remained comparable. Furthermore one can note that the pseudo-value approach was not better than the models based on proportional hazards. To illustrate the behavior of each model to this misspecification, Figure 6a depicts the time-varying coefficient $\eta_{1,k} * \log(1 + t)$ used in the data generation and the time-invariant parameters estimated in the joint and two-stage landmark CS PH models for one random replicate. The landmark model permitted to obtain estimated parameters closer to the generated one (except for $s = 8$ because only 8 and 13 subjects experienced the event between 8 and $8 + w$ for $w = 1.5$ and $w = 3$, respectively) but these estimates had also large variances because of the considered information which might explain the non superiority of landmark approaches to this misspecification.

[Figure 4 about here.]

4.2.4 Case 4: Misspecification of the longitudinal trajectory of the marker

The last case studied the performances of the prediction models when the longitudinal trend of the marker was misspecified. Data were generated using a joint model with a biphasic shape of the marker:

$$\begin{cases} Y_i(t) = m_i(t) + \epsilon_i(t) \\ = (\beta_0 + \beta_{0,X}X_i + b_{i0}) + (\beta_1 + \beta_{1,X}X_i + b_{i1})((1+t)^{-1.2} - 1) + (\beta_2 + \beta_{2,X}X_i + b_{i2})t + \epsilon_i(t), \\ \lambda_i^k(t) = \lambda_{k,0}(t) \exp \left\{ \gamma_k X_i + \eta_{1,k} m_i(t) + \eta_{2,k} \frac{\delta m_i(t)}{\delta t} \right\}. \end{cases}$$

For the estimation of the predicted probabilities of event using joint and two-stage landmark models, we considered a linear trajectory over time for the marker. As shown in Figure 6b, the degree of misspecification of the longitudinal marker trend was severe but it was made on purpose to clearly show the impact of such misspecification.

Figure 5 displays the boxplots of differences in MSE for the 8 pairs (s, w) . The landmark models performed much better than the joint models for landmark times $s = 1, 3, 5$; at landmark time $s = 8$, performances of joint and landmark models became roughly similar. Such result was expected. The joint model incorrectly assumed a linear trajectory for the marker on the whole follow-up while the landmark model, by considering only the longitudinal information collected until s , assumed a linear trajectory only until s which was more realistic at earliest landmark times even if still far from being well specified.

Figure 6b illustrates the differences in the predicted current values of the marker used in the estimated models to predict the risk of recurrence for a hypothetical subject \star with $b_\star = 0$ and $X_\star = 2.04$ in a randomly selected replication. The difference between the predicted levels of the marker are very different at the earliest landmark times between the joint and landmark models while they converge to roughly the same value at $s = 8$. Moreover the joint model actually uses the predicted current level of the marker rather than the predicted marker value in s which does not necessarily follows the generated path.

[Figure 5 about here.]

To explore whether such differences were due to the severe misspecification of our example, we considered a second longitudinal marker trend in Section 3.1 of the Web Appendix. This supplementary case considered a small degree of misspecification of the longitudinal marker by considering some slight fluctuations with splines in the generation model compared to the well-specified case 1. Although slightly misspecified, the superiority of joint model over landmark approaches previously found in case 1 almost completely disappeared. This confirmed the high sensitivity to any kind of misspecification of the marker trajectory in the joint model.

[Figure 6 about here.]

5 Discussion

With the development of personalized medicine, it is important to provide valid and powerful tools to clinicians for the computation of individual probabilities of specific events such as landmark conditional cumulative incidences. These predictions are expected to be used in clinical practice, notably to adapt individual strategies of treatment or to plan the patient-specific optimal screening time in clinical trials.

Several authors (Maziarz et al., 2017; Rizopoulos, 2011) already proposed estimators of the individual landmark conditional cumulative incidence $\pi_{\star}^k(s, w)$, but surprisingly none was formally validated using simulation studies.

Our first objective was thus to formally define the quantity of interest $\pi_{\star}^k(s, w)$ and provide correct estimators (along with 95% confidence interval) both for the landmarking and the joint modelling approaches and properly validate them by comparing generated and estimated expressions of $\pi_{\star}^k(s, w)$. The computation of the generated quantity of interest was not obvious because it involved an integral over the latent structure shared by the longitudinal process and the survival process, the data being generated from a joint model. Note that in some papers, such quantity of interest is not correctly defined (Barrett and Su, 2017; Sweeting et al., 2016). The marginal estimator from the joint model obtained very good performance in general whereas it was showed that the conditional estimator from the joint model necessitates sufficient individual longitudinal information collected until the prediction time.

Uncertainty around the individual predictions is essential for the decision making in clinical practice. In the landmark approach no solution was ever proposed, and we suspected the usual definition of the confidence intervals in the joint modelling framework to be incorrect. We thus proposed methods to take into account properly the variability around the predictions for each approach and showed that they correctly assessed the uncertainty around the individual predictions. Compared to the joint model, the estimator based on the two-stage landmark cause-specific proportional hazards model confirmed its expected poor efficiency, with wide confidence intervals when only a few subjects experienced the event in the prediction window.

A series of papers showed comparisons of prediction models in dynamic predictions (Goldstein et al., 2017; Huang et al., 2016; Sweeting et al., 2016) but none evaluated their robustness to misspecifications although most proposed methods were parametric. Our second objective was thus to properly compare the landmark models and the joint model through several cases of well- and mis-specification. In case of correctly specified model, as expected, we found that the joint model performed better than the landmark models. In case of misspecification of the dependence structure between the longitudinal process and the survival process, the difference of performances between approaches did not change but the global performance of models was much worse. Regarding the PH assumption, the impact of its violation on the estimators derived from the joint model was limited, suggesting that the violation of the PH assumption should be extreme to entail a tangible impact on the estimated cumulative incidences in the joint model.

Finally, we showed that the correct specification of the marker trajectory was essential to provide good predictions with joint models, and with landmark models at distant prediction times. We demonstrated the lack of performance of the joint model in a severe case of misspecification to illustrate the limit but we also found in Web Appendix that even a slight misspecification of the trajectory (usually considered as acceptable) impacted the predictive performances of the models, and eliminated for example the gain of using the joint model over the landmark model at shorter landmark times or when the horizon time increases.

Note that for the comparison of the prediction models in terms of prediction accuracy, we focused on Mean Square Errors (MSE) rather than Brier scores. Indeed the Brier score is only an approximation of the MSE and the simulation study context enabled us to compute the generated quantities of interest for all subjects. A supplementary analysis (in Web Appendix 3.2) considered the Areas Under ROC Curves (AUC). These additional results that permitted comparing the prediction models in terms of discrimination were in agreement with those obtained using MSE.

To conclude with recommendations, we emphasize the need to carefully define and validate the estimator of the quantity of interest and its uncertainty estimator. The several cases of misspecifica-

tion warned us on the necessity to precisely specify the dependence structure between the longitudinal marker dynamics and the risk of event. Finally, the specification of the longitudinal marker trend should be studied with extreme care, especially when using joint modelling. Researchers should be warned that the use of sophisticated methods such as the joint models may allow obtaining accurate and efficient estimators only when they are correctly specified. Otherwise, estimators might be off the mark. Landmark models seem less sensitive to the misspecification of the longitudinal marker trajectory but are as sensitive as joint models regarding the dependence structure. In addition, they provide considerably less efficient estimators and may induce convergence problems, notably when the landmark time increases and thus the considered information is too poor.

Acknowledgements

The authors thank warmly Boris P. Hejblum for his valuable advice and assistance. This work was supported by a joint grant from INSERM and Région Aquitaine, a grant from the Institut OpenHealth and a grant from the Réseau Franco-Néerlandais. Computer time for this study was provided by the computing facilities MCIA (Mésocentre de Calcul Intensif Aquitain) of the Université de Bordeaux and of the Université de Pau et des Pays de l'Adour.

Supplementary Materials

A Web Appendix may be found in the source package of this article on arXiv. Detailed examples of the code can be found at <https://github.com/LoicFerrer> for practical use.

References

Andersen, P. K., Borgan, O., Gill, R. D., and Keiding, N. (1993). *Statistical Models Based On Counting Processes*. Springer-Verlag, New York.

Andersen, P. K. and Pohar Perme, M. (2010). Pseudo-observations in survival analysis. *Statistical Methods in Medical Research* **19**, 71–99.

Barrett, J. and Su, L. (2017). Dynamic predictions using flexible joint models of longitudinal and time-to-event data. *Statistics in Medicine* **36**, 1447–1460.

Breslow, N. E. (1972). Discussion of Professor Cox's paper. *Journal of the Royal Statistical Society, Series B* **34**, 216–217.

Cox, D. R. (1972). Regression models and life tables (with discussion). *Journal of the Royal Statistical Society, Series B* **34**, 187–220.

Crowther, M. J. and Lambert, P. C. (2013). Simulating biologically plausible complex survival data. *Statistics in Medicine* **32**, 4118–4134.

Ferrer, L., Rondeau, V., Dignam, J., Pickles, T., Jacqmin-Gadda, H., and Proust-Lima, C. (2016). Joint modelling of longitudinal and multi-state processes: application to clinical progressions in prostate cancer. *Statistics in Medicine* **35**, 3933–3948.

Fine, J. P. and Gray, R. J. (1999). A proportional hazards model for the subdistribution of a competing risk. *Journal of the American Statistical Association* **94**, 496–509.

Goldstein, B. A., Pomann, G. M., Winkelmayer, W. C., and Pencina, M. J. (2017). A comparison of risk prediction methods using repeated observations: an application to electronic health records for hemodialysis. *Statistics in Medicine* **36**, 2750–2763.

Huang, X., Yan, F., Ning, J., Feng, Z., Choi, S., and Cortes, J. (2016). A two-stage approach for dynamic prediction of time-to-event distributions. *Statistics in Medicine* **35**, 2167–2182.

Jewell, N. P. and Nielsen, J. P. (1993). A framework for consistent prediction rules based on markers. *Biometrika* **80**, 153–164.

Maziarz, M., Heagerty, P., Cai, T., and Zheng, Y. (2017). On longitudinal prediction with time-to-event outcome: Comparison of modeling options. *Biometrics* **73**, 83–93.

Nicolaie, M., van Houwelingen, J., de Witte, T., and Putter, H. (2013). Dynamic pseudo-observations: A robust approach to dynamic prediction in competing risks. *Biometrics* **69**, 1043–1052.

Proust-Lima, C. and Taylor, J. M. (2009). Development and validation of a dynamic prognostic tool for prostate cancer recurrence using repeated measures of posttreatment PSA: a joint modeling approach. *Biostatistics* **10**, 535–549.

Proust-Lima, C., Taylor, J. M., Williams, S. G., Ankerst, D. P., Liu, N., Kestin, L. L., Bae, K., and Sandler, H. M. (2008). Determinants of change in prostate-specific antigen over time and its association with recurrence after external beam radiation therapy for prostate cancer in five large cohorts. *International Journal of Radiation Oncology Biology Physics* **72**, 782–791.

Rizopoulos, D. (2011). Dynamic predictions and prospective accuracy in joint models for longitudinal and time-to-event data. *Biometrics* **67**, 819–829.

Rizopoulos, D. (2012). *Joint Models for Longitudinal and Time-to-Event Data: with Applications in R*. Chapman & Hall/CRC, Boca Raton.

Rizopoulos, D., Taylor, J. M., Van Rosmalen, J., Steyerberg, E. W., and Takkenberg, J. J. (2015). Personalized screening intervals for biomarkers using joint models for longitudinal and survival data. *Biostatistics* **17**, 149–164.

Scheike, T. H., Zhang, M.-J., and Gerds, T. A. (2008). Predicting cumulative incidence probability by direct binomial regression. *Biometrika* **95**, 205–220.

Sène, M., Taylor, J. M., Dignam, J. J., Jacqmin-Gadda, H., and Proust-Lima, C. (2016). Individualized dynamic prediction of prostate cancer recurrence with and without the initiation of a second treatment: Development and validation. *Statistical Methods in Medical Research* **25**, 2972–2991.

Sinnott, J. A. and Cai, T. (2016). Inference for survival prediction under the regularized Cox model. *Biostatistics* **17**, 692–707.

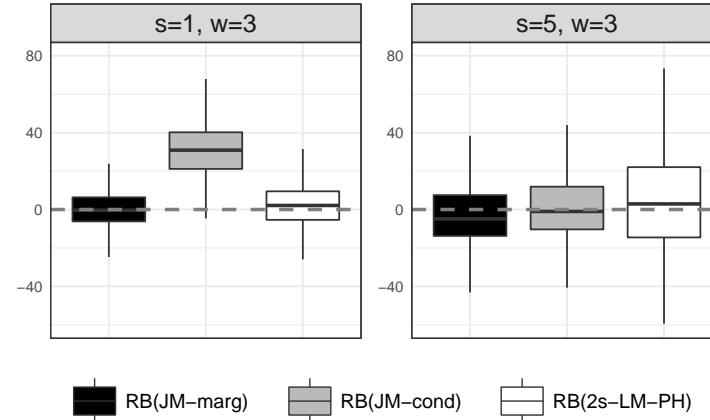
Suresh, K., Taylor, J. M., Spratt, D. E., Daignault, S., and Tsodikov, A. (in press, 2017). Comparison of joint modeling and landmarking for dynamic prediction under an illness-death model. *Biometrical Journal* .

Sweeting, M. J., Barrett, J. K., Thompson, S. G., and Wood, A. M. (in press, 2016). The use of repeated blood pressure measures for cardiovascular risk prediction: a comparison of statistical models in the ARIC study. *Statistics in Medicine* .

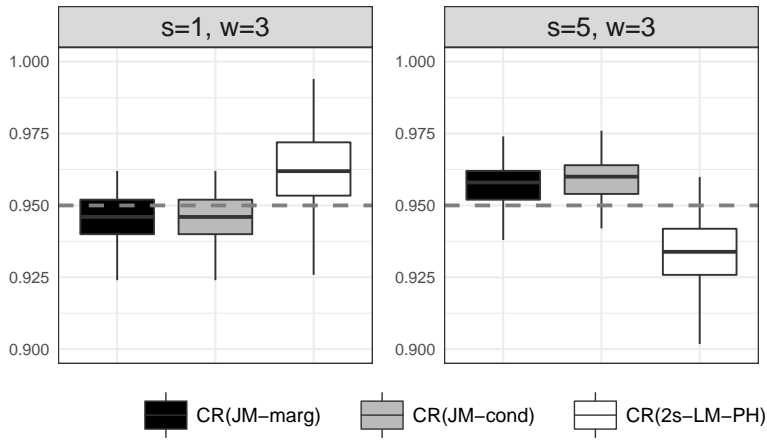
Taylor, J. M., Park, Y., Ankerst, D. P., Proust-Lima, C., Williams, S., Kestin, L., Bae, K., Pickles, T., and Sandler, H. (2013). Real-time individual predictions of prostate cancer recurrence using joint models. *Biometrics* **69**, 206–213.

Tsiatis, A. A. and Davidian, M. (2004). Joint modeling of longitudinal and time-to-event data: an overview. *Statistica Sinica* **14**, 809–834.

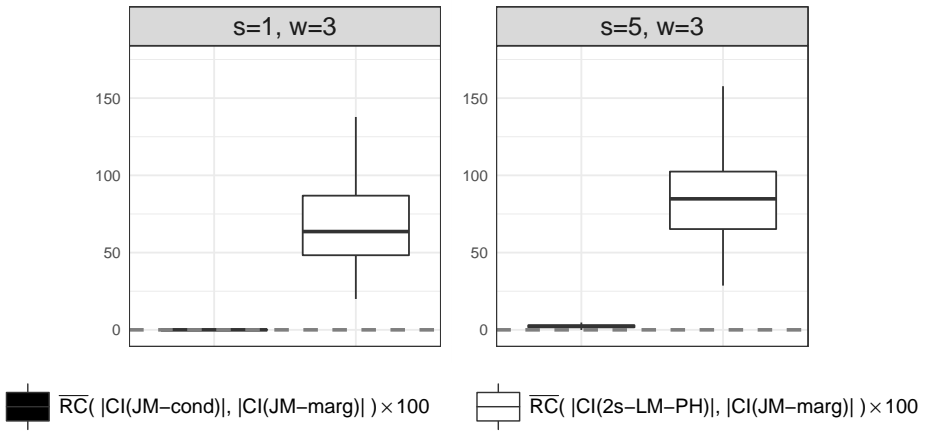
Van Houwelingen, H. C. (2007). Dynamic prediction by landmarking in event history analysis. *Scandinavian Journal of Statistics* **34**, 70–85.



(a) Evaluation of the estimators: distribution over the individuals $\star = 1, \dots, N(s)$ of the relative bias (RB, in %). The dashed line represents the 0.



(b) Evaluation of the confidence intervals: distribution over the individuals $\star = 1, \dots, 200$ of the coverage rates (CR) for the 95% confidence intervals of $\pi_{\star}^{\text{Rec.}}(s, w; \theta)$. The dashed line represents the 0.95.



(c) Evaluation of the estimator efficiency: distribution over the individuals $\star = 1, \dots, 200$ of the mean relative changes (\overline{RC} , in %) of the 95% confidence interval (CI) widths. The dashed line represents the 0.

Figure 1 – Evaluation of the estimators in terms of relative bias (a), coverage rates (b) and mean relative changes of the confidence intervals widths (c). Considered are the marginal estimator and the conditional estimator from the joint model (denoted JM-marg and JM-cond, respectively) and the estimator based on the two-stage cause-specific landmark model (denoted 2s-LM-PH).

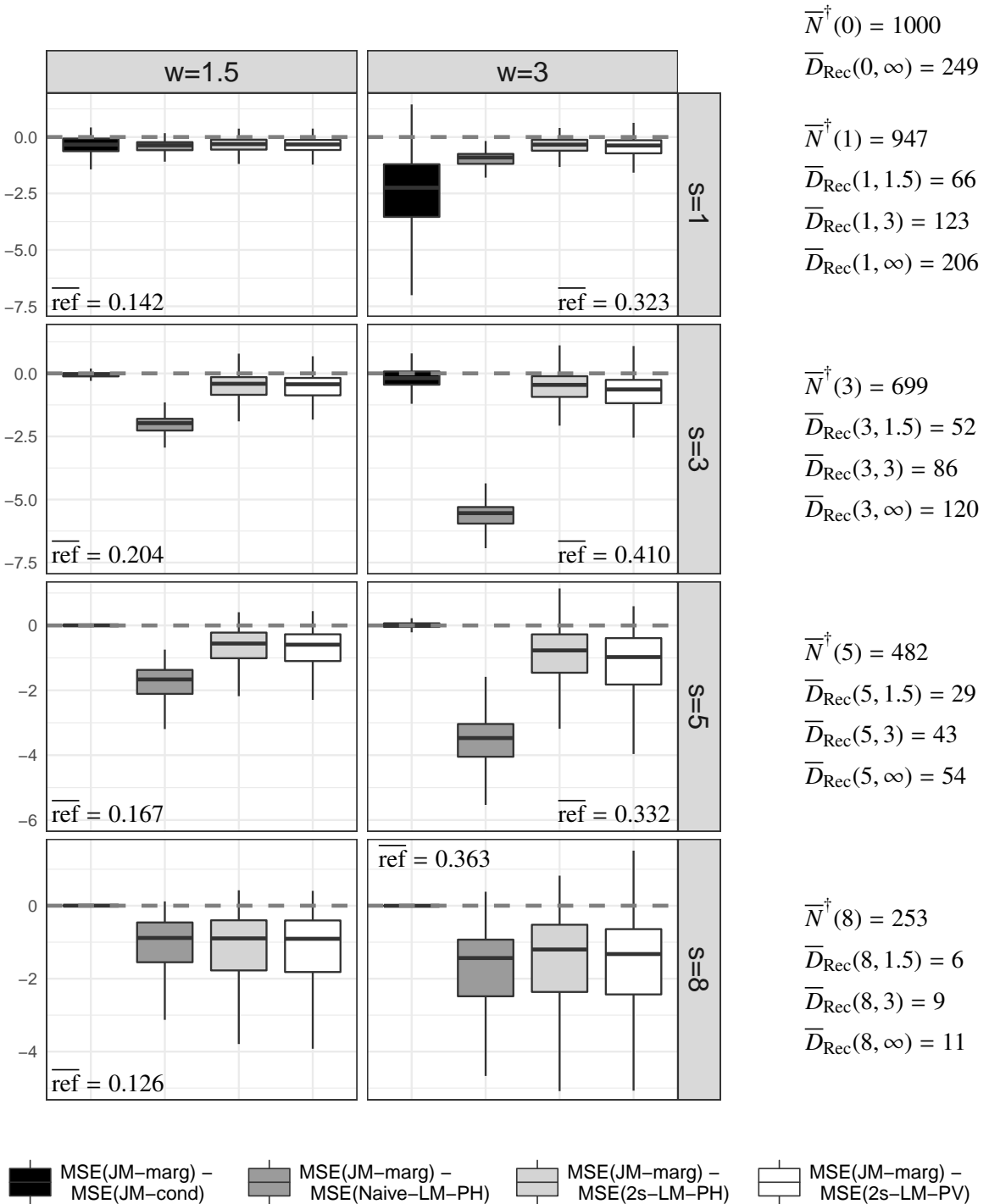


Figure 2 – Boxplots of the differences ($\times 1000$) of Mean Square Error of prediction (MSE) between the marginal estimator from the joint model (denoted JM-marg) and alternatives in the case of correct specification of the joint model (case 1). Considered are the conditional estimator from the joint model (JM-cond), the estimators from cause-specific landmark models using a two-stage or naive approach (2s-LM-PH and Naive-LM-PH, respectively) and the two-stage pseudo value model (2s-LM-PV). The distributions are depicted over $R = 499, 494, 486, 389$ replicates for 4 landmark times $s = 1, 3, 5, 8$ respectively, with 2 considered horizons $w = 1.5$ and $w = 3$. ref denotes the mean MSE ($\times 1000$) using the marginal estimator from the joint model for each (s, w) . $\overline{N}^\dagger(s)$ is the mean number of subjects at risk at s and $\overline{D}_{\text{Rec}}(s, w)$ is the mean number of recurrences occurred between s and $s + w$.

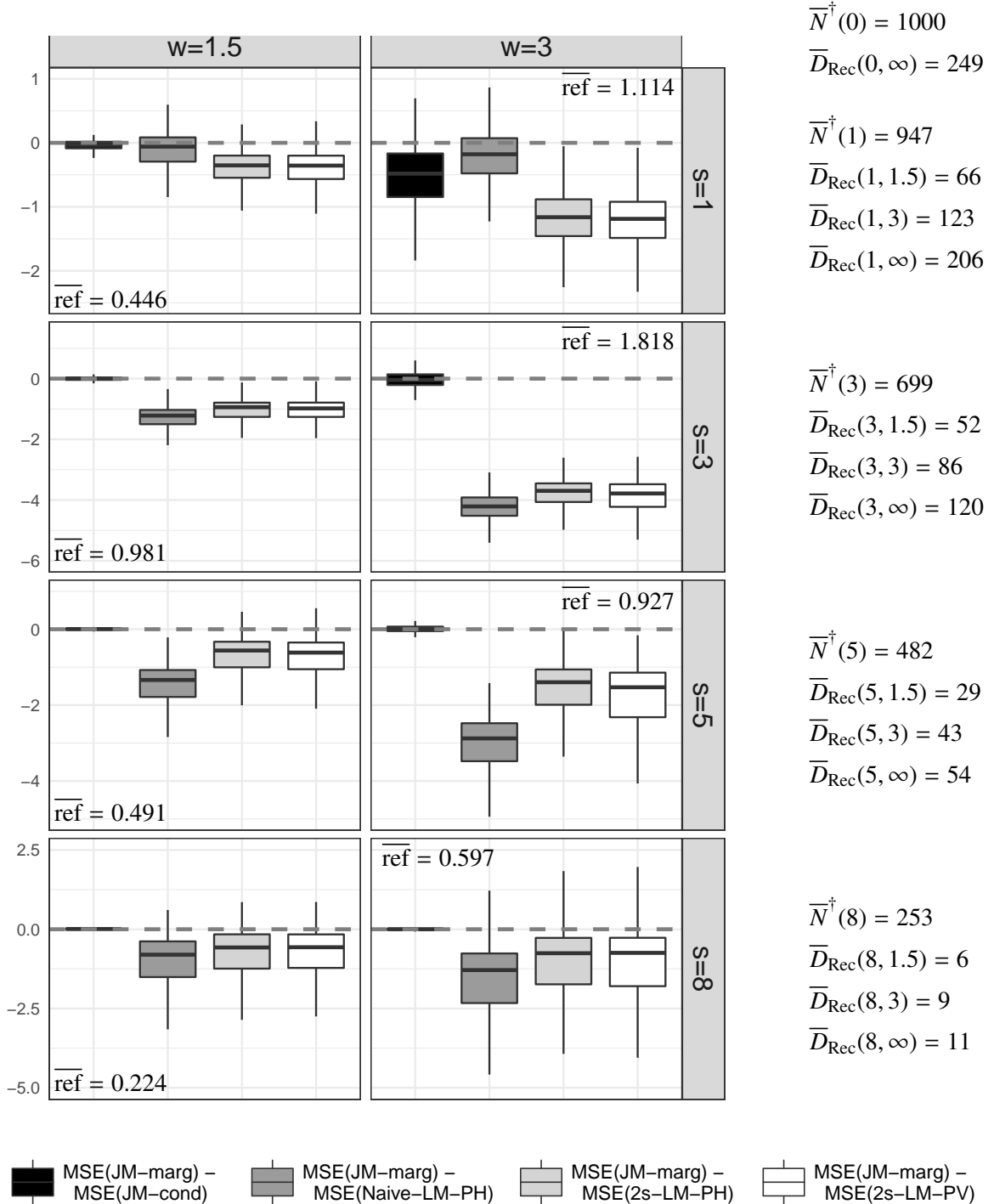


Figure 3 – Boxplots of the differences ($\times 1000$) of Mean Square Error of prediction (MSE) between the marginal estimator from the joint model (denoted JM-marg) and alternatives in the case of misspecification of the dependence function (case 2). Considered are the conditional estimator from the joint model (JM-cond), the estimators from cause-specific landmark models using a two-stage or naive approach (2s-LM-PH and Naive-LM-PH, respectively) and the two-stage pseudo value model (2s-LM-PV). The distributions are depicted over $R = 499, 498, 497, 428$ replicates for 4 landmark times $s = 1, 3, 5, 8$ respectively, with 2 considered horizons $w = 1.5$ and $w = 3$. ref denotes the mean MSE ($\times 1000$) using the marginal estimator from the joint model for each (s, w) . $\overline{N}^\dagger(s)$ is the mean number of subjects at risk at s and $\overline{D}_{\text{Rec}}(s, w)$ is the mean number of recurrences occurred between s and $s + w$.

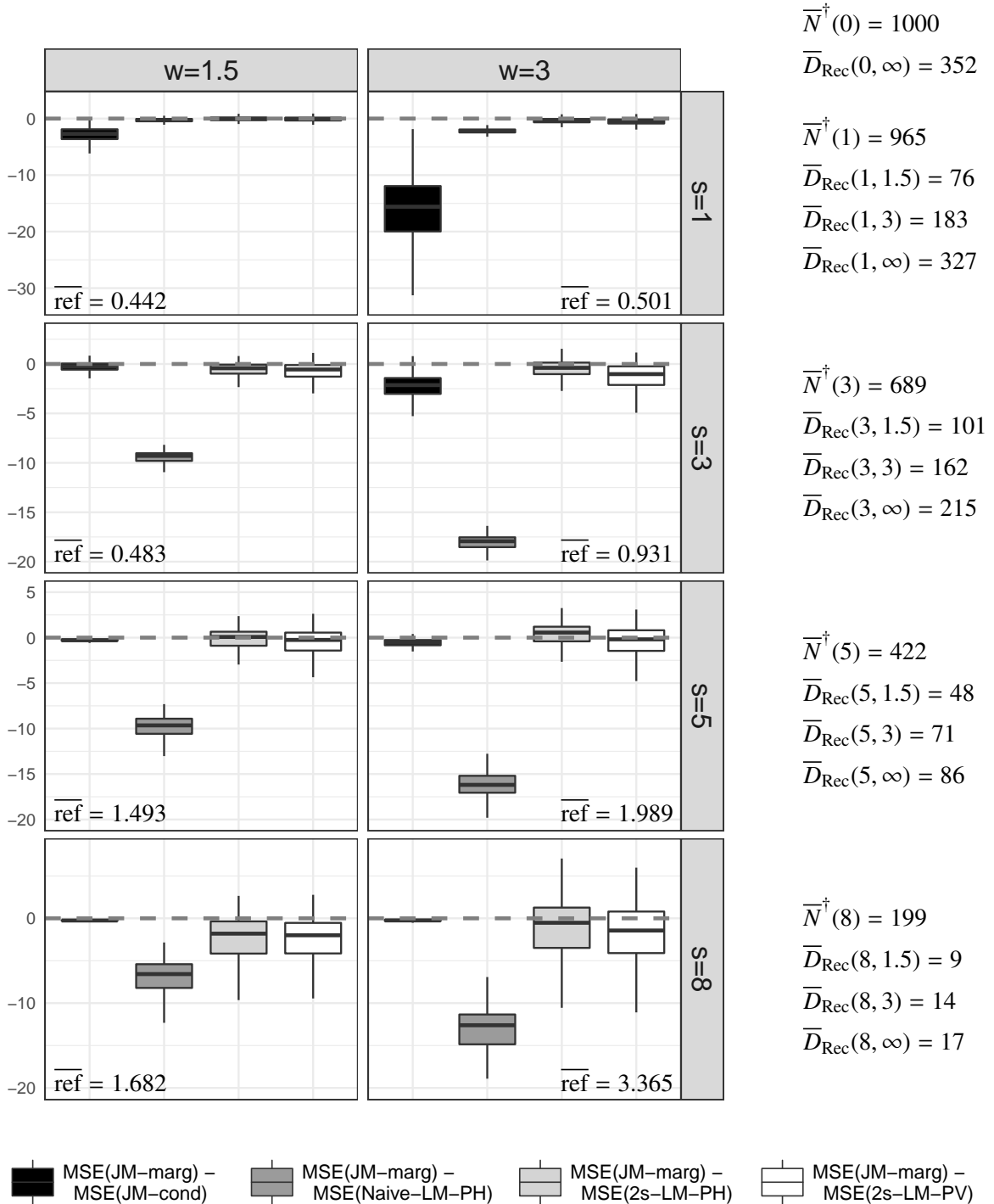


Figure 4 – Boxplots of the differences ($\times 1000$) of Mean Square Error of prediction (MSE) between the marginal estimator from the joint model (denoted JM-marg) and alternatives in the case of substantial violation of the PH assumption (case 3). Considered are the conditional estimator from the joint model (JM-cond), the estimators from cause-specific landmark models using a two-stage or naive approach (2s-LM-PH and Naive-LM-PH, respectively) and the two-stage pseudo value model (2s-LM-PV). The distributions are depicted over $R = 485, 326, 294, 188$ replicates for 4 landmark times $s = 1, 3, 5, 8$ respectively, with 2 considered horizons $w = 1.5$ and $w = 3$. ref denotes the mean MSE ($\times 1000$) using the marginal estimator from the joint model for each (s, w) . $\overline{N}^\dagger(s)$ is the mean number of subjects at risk at s and $\overline{D}_{\text{Rec}}(s, w)$ is the mean number of recurrences occurred between s and $s + w$.

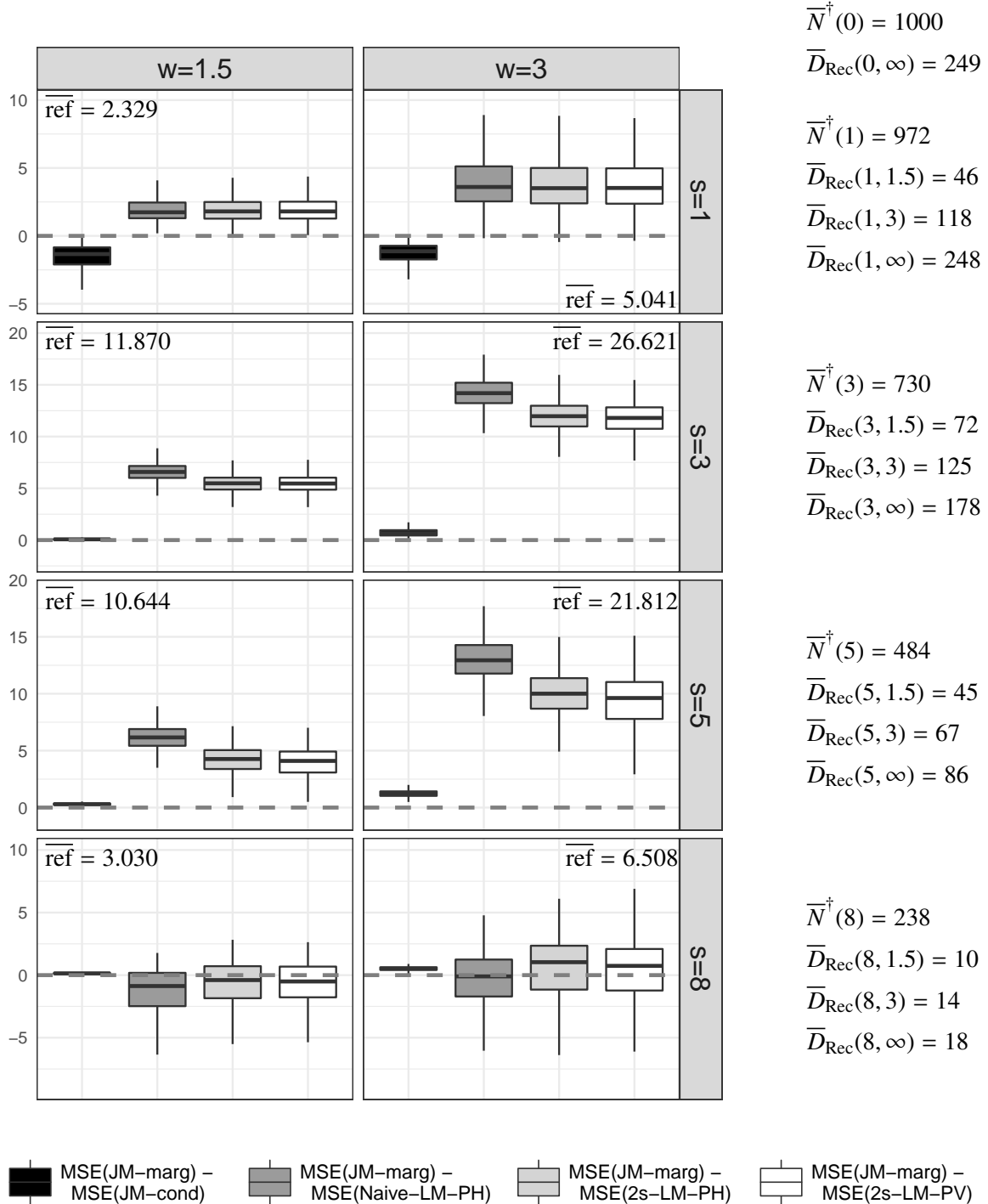
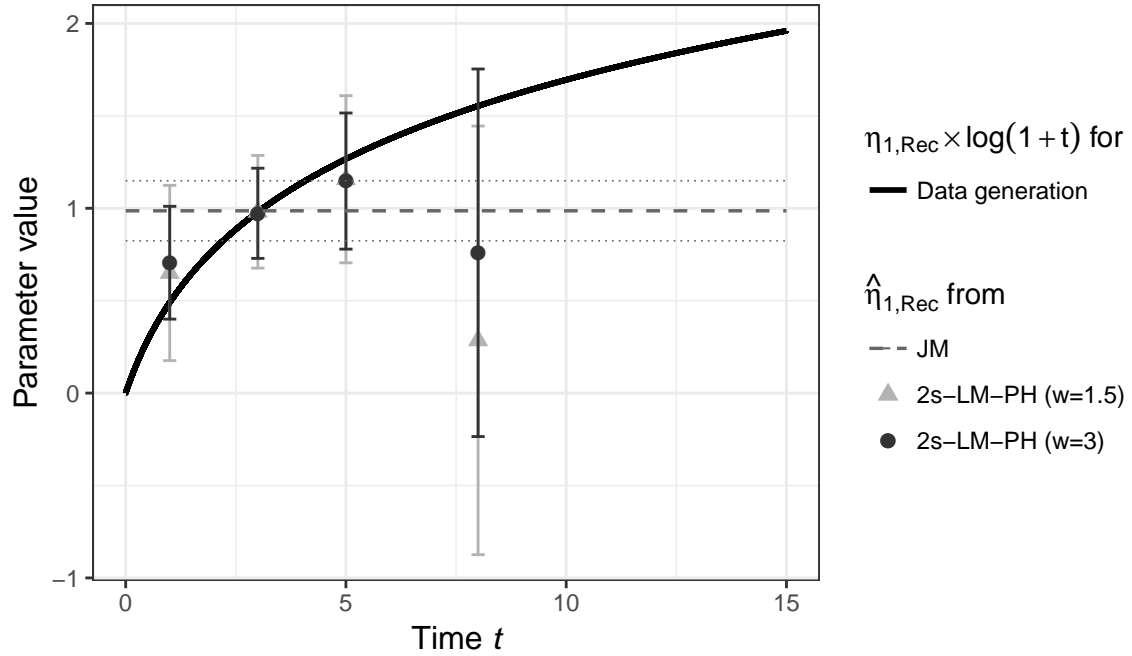
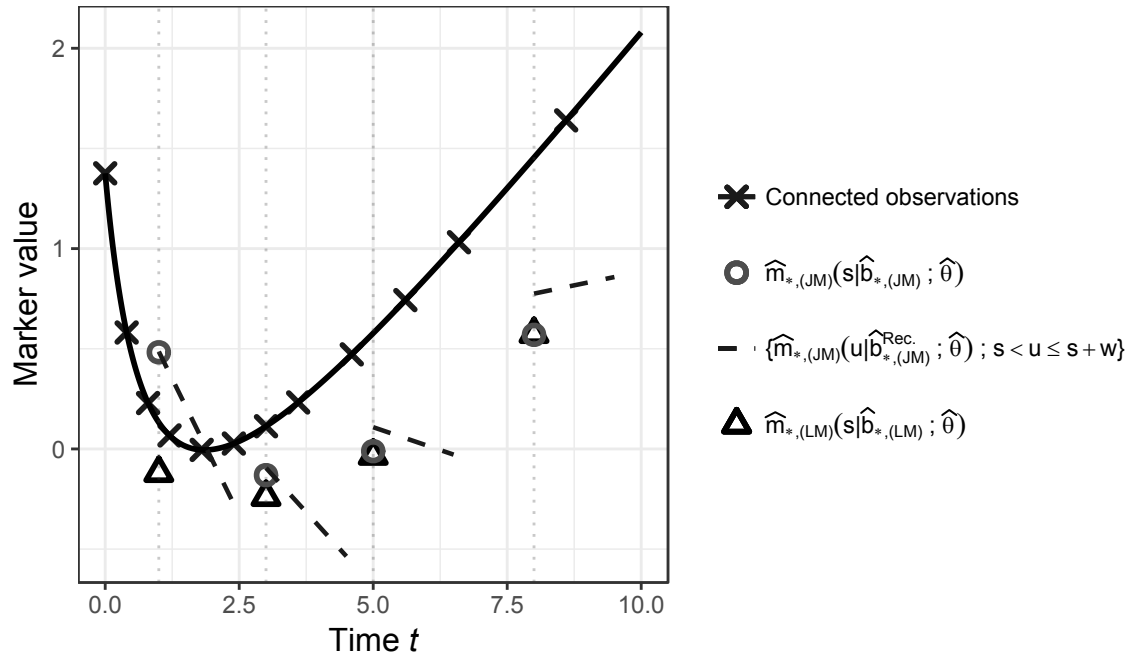


Figure 5 – Boxplots of the differences ($\times 1000$) of Mean Square Error of prediction (MSE) between the marginal estimator from the joint model (denoted JM-marg) and alternatives in the case of substantial misspecification of the longitudinal marker trajectory (case 4). Considered are the conditional estimator from the joint model (JM-cond), the estimators from cause-specific landmark models using a two-stage or naive approach (2s-LM-PH and Naive-LM-PH, respectively) and the two-stage pseudo value model (2s-LM-PV). The distributions are depicted over $R = 500, 496, 476, 357$ replicates for 4 landmark times $s = 1, 3, 5, 8$ respectively, with 2 considered horizons $w = 1.5$ and $w = 3$. ref denotes the mean MSE ($\times 1000$) using the marginal estimator from the joint model for each (s, w) . $\overline{N}^\dagger(s)$ is the mean number of subjects at risk at s and $\overline{D}_{\text{Rec}}(s, w)$ is the mean number of recurrences occurred between s and $s + w$.



(a) Example of log relative risk of recurrence associated with the current marker level in the generation data with a time-varying effect ($\eta_{1,\text{Rec}} \times \log(1 + t)$). Are also depicted the estimated effects ($\widehat{\eta}_{1,\text{Rec}}$) in the joint model (JM) and the two-stage cause specific landmark models (2s-LM-PH) with horizons $w = 1.5$ and $w = 3$, and their associated estimated 95% confidence intervals.



(b) Example of nonlinear marker trajectory considered in the generation data for a mean subject \star with $b_{\star} = 0$ and $X_{\star} = 2.04$. Are also represented the current values of the marker actually predicted in the estimation models (denoted $\widehat{m}_{*}(\text{JM})$ for the joint model and $\widehat{m}_{*}(\text{LM})$ for the two-stage landmark models) which are based for the joint model on $\widehat{b}_{*,\text{(JM)}} = \arg \max_b f(b|T_{\star} > s, \mathcal{Y}_{\star}(s), X_{\star}; \widehat{\theta})$ in the denominator of the conditional estimator definition and $\widehat{b}_{*,\text{(JM)}}^{\text{Rec.}} = \arg \max_b f(b|T_{\star} > s, \delta_{\star} = \text{Rec.}, \mathcal{Y}_{\star}(s), X_{\star}; \widehat{\theta})$ in the numerator (see formula in Section 1.2 of the Web Appendix), and for the two-stage landmark models on $\widehat{b}_{*,\text{(LM)}} = \mathbb{E}(b_{\star}|\mathcal{Y}_{\star}(s), X_{\star}; \widehat{\theta})$.

Figure 6 – Illustrative examples of the model behaviors on a randomly selected replicate for misspecified cases 3 and 4.